Research Square

Preprints are preliminary reports that have not undergone peer review.
They should not be considered conclusive, used to inform clinical practice,
or referenced by the media as validated information.

Carbon Nanofiber Encapsulated High-Entropy Phosphides for Efficient Alkaline Water Splitting

Yi Shen
Changzhou University
Yiming Zhang
Changzhou University
Haotian Sun
Changzhou University
Xiangqun Zhuge
Changzhou University
Kang Liang
Changzhou University
Jianbin Li
Changzhou University
Peng Wei
Changzhou University
Shunyi Yang
BTR (Jiangsu) New Material Technology Co.,Ltd
Yurong Ren
ryrchem@cczu.edu.cn
Changzhou University

Research Article

Keywords: Water splitting, High-entropy phosphides, Electrocatalysts, Electrospinning

Posted Date: November 18th, 2026

DOI: https://doi.org/10.21203/rs.3.rs-11638302/v1

License: This work is licensed under a Creative Commons Attribution 4.0 International License.
Read Full License

Additional Declarations: No competing interests reported.

Carbon Nanofiber Encapsulated High-Entropy Phosphides for Efficient Alkaline Water Splitting

Yi Shen[a, †], Yiming Zhang[a, †], Haotian Sun[a], Xiangqun Zhuge[a], Kang Liang[a], Jianbin Li[a], Peng Wei[a, *], Shunyi Yang[b, *], and Yurong Ren[a, *]

[a] *School of Materials Science and Engineering, Changzhou University, Changzhou 213164, China*

[b] *BTR (Jiangsu) New Material Technology Co.,Ltd., Changzhou 213299, China*

*Corresponding author: weipeng@cczu.edu.cn (P. Wei); yangshunyi@btrchina.com (S.Y. Yang); *ryrchem@cczu.edu.cn* (Y.R. Ren).

[†]Y. S. and Y.M. Z. contributed equally to this work.

Abstract

Transition-metal phosphides (TMPs) have attracted extensive attention as promising electrocatalysts for water splitting owing to their distinctive electronic structures, high natural abundance, low cost, and favorable electrochemical activity. Although substantial progress has been achieved in developing high-performance TMP electrocatalysts, most reported systems still suffer from hazardous, complicated synthetic routes that rely on toxic phosphorus precursors, together with insufficient intrinsic activity and poor stability. Herein, we report a green and scalable strategy to fabricate carbon-nanofiber-encapsulated high-entropy phosphides (MFeCoNiP@NCNFs, M=Cr/Mn/Mo/Cu). The synthesis employs non-toxic, renewable phytic acid as the phosphorus source, combining electrospinning with subsequent thermal treatment. The carbon-nanofiber skeleton provides continuous electron-transport pathways, confines phosphide nanoparticles to suppress agglomeration, and enables uniform incorporation of additional metal components for electronic-structure modulation. Benefiting from the high-entropy effect and Cr

doping, the optimized CrFeCoNiP@NCNFs delivers outstanding bifunctional electrocatalytic activity and stability in alkaline media, exhibiting low overpotentials of 133 mV for the hydrogen evolution reaction (HER) and 309 mV for the oxygen evolution reaction (OER) at 10 $mA \cdot cm^{-2}$.

Keywords: Water splitting; High-entropy phosphides; Electrocatalysts; Electrospinning

1. Introduction

Hydrogen is a carbon-neutral, zero-emission energy carrier and is widely regarded as a promising alternative to fossil fuels [1-3]. Electrochemical overall water-splitting for hydrogen production represents a clean energy-cycling technology that comprises the oxygen evolution reaction (OER) and hydrogen evolution reaction (HER). It is recognized as one of the simplest, most environmentally benign, and most efficient hydrogen-production technologies [4-10]. Nevertheless, reaction energy barriers raise the practical water-splitting voltage far above the theoretical value. Therefore, catalysts are required to reduce energy consumption during energy conversion and improve energy-conversion efficiency. State-of-the-art electrocatalysts are mainly based on precious metals (Pt, Ru, Ir), yet their practical deployment is severely restricted by high cost, limited reserves, and unsatisfactory stability [11-13]. Accordingly, exploring non-precious-metal electrocatalysts with high abundance, low cost, and high efficiency is of great practical significance [14,15]. Bifunctional catalysts are particularly attractive for further cutting catalyst costs.

In recent years, considerable efforts have been devoted to developing low-cost, high-performance electrocatalysts based on transition-metal materials, including transition-metal carbides, oxides, nitrides, sulfides, selenides, and phosphides [16-28]. Among these candidates, transition-metal phosphides (TMPs) stand out as promising electrocatalysts by virtue of their unique electronic structures and excellent mechanical and electrochemical properties, showing great potential toward alkaline HER and OER [29-32]. However, single-component transition-metal phosphides

generally possess limited intrinsic active sites, and precise tuning of intermediate-adsorption energies remains challenging. It is therefore critical to increase active-site exposure and construct efficient ion- and electron-transport pathways. Constructing high-entropy phosphides by introducing multiple metal atoms offers a viable solution. The synergistic interactions among diverse metal atoms and high-entropy effects (including severe lattice distortion, sluggish atomic diffusion, and the cocktail effect) trigger electron redistribution, modulate the d-band-center position, and boost water-electrolysis catalytic activity [33-36]. For instance, Cai et al. prepared fourteen-element nanoporous ultra-high-entropy alloys with excellent water-splitting electrocatalytic performance [37]. Zhang and co-workers reported hollow multilayer heterostructured CoFeP-based catalysts containing abundant active sites, which exhibited remarkable bifunctional activity in alkaline electrolytes [38]. Even so, most of these syntheses utilize hypophosphite precursors, inevitably generating toxic PH_3 gas during thermal processing. To resolve this issue, developing low-cost, non-toxic phosphorus sources that avoid corrosive-gas release is fundamentally important. Sun et al. also adopted phytic acid as an auxiliary reagent to fabricate ultra-small NiCoP confined within P, N-co-doped carbon nanofibers, which exhibited good bifunctional performance [39]. Despite these advances, phosphide nanoparticles obtained from green phosphorus sources still suffer from uncontrolled grain growth, severe agglomeration, and unsatisfactory long-term stability, limiting active-site exposure. Consequently, confining phosphide nanoparticles inside a protective, conductive matrix to reduce particle size and enhance stability deserves further investigation.

Electrospinning is a versatile technique for fabricating one-dimensional nanofiber materials. Carbon sources, metal precursors, and phosphorus sources can be mixed at the molecular level and converted into carbon-nanofiber-encapsulated nanostructures upon heat treatment. Herein, we report the green fabrication of carbon-nanofiber-encapsulated high-entropy phosphides via electrospinning followed by thermal annealing. Phytic acid serves as the non-toxic phosphorus source, polyacrylonitrile (PAN) as the carbon source, and melamine as an extra nitrogen source. The one-dimensional carbon-nanofiber skeleton establishes continuous

electron-transport pathways and physically suppresses over-growth and agglomeration of phosphide nanoparticles. Meanwhile, high-entropy design enables uniform incorporation of multiple metal components to regulate electronic structures.

After doping FeCoNiP with transition-metal species (Cr/Mn/Mo/Cu), the optimized CrFeCoNiP@NCNFs delivers HER and OER overpotentials of 133 mV and 309 mV at 10 $mA \cdot cm^{-2}$. Such performance originates from increased phosphorus-vacancy concentration, enlarged electrochemically active surface area, and reduced charge-transfer resistance. Energy shifts of metal and phosphorus sites displace the d-band centers relative to the Fermi level, optimizing intermediate adsorption and improving catalytic performance. Impressively, when CrFeCoNiP@NCNFs is assembled as both anode and cathode for overall water-splitting, the electrolyzer only requires 1.89 V to achieve 10 $mA \cdot cm^{-2}$ and can operate stably for 12 h. This work not only develops efficient bifunctional electrocatalysts, but also expands green synthetic routes toward nanoscale high-entropy phosphides, paving the way for their large-scale practical implementation.

2. Experimental section

2.1. Reagents

All reagents were of analytical grade and used as received without further purification. Phytic acid ($C_6H_{18}O_{24}P_6$), melamine ($C_3H_6N_6$), potassium hydroxide (KOH), anhydrous copper chloride ($CuCl_2$), molybdenyl acetylacetonate ($C_{10}H_{14}MoO_6$), nickel chloride hexahydrate ($NiCl_2 \cdot 6H_2O$), ferric chloride ($FeCl_3$), cobalt chloride hexahydrate ($CoCl_2 \cdot 6H_2O$), manganese chloride ($MnCl_2$), ammonium molybdate tetrahydrate ($(NH_4)_6Mo_7O_{24} \cdot 4H_2O$), N,N-dimethylformamide (DMF), polyacrylonitrile (PAN), cobalt acetylacetonate ($C_{10}H_{16}CoO_4$), ammonium hypophosphite ($NH_4H_2PO_2$), and deionized water were purchased from Sinopharm Chemical Reagent (Shanghai, China). Anhydrous ethanol and commercial 20 wt% Pt/C catalyst were obtained from Aladdin Reagent (Shanghai, China).

2.2. Sample synthesis

FeCoNiP nanofibers were synthesized via a simple electrospinning process and subjected to high-temperature heat treatment. 0.25 mmol of iron chloride, cobalt chloride, and nickel chloride were added to 10 mL of DMF, followed by the addition of 0.825 g of phytic acid and 0.8 g of polyacrylonitrile powder. The mixture was stirred for 24 hours on a magnetic stirrer to obtain a transparent spinning solution. The solution was then transferred into a 10 mL syringe, and a 21-gauge needle was selected. The spinning voltage was set at 20 kV, and the feed rate was 0.8 mL/h. The precursor fiber membrane was produced via electrospinning.

As spun fiber mat was recorded as FeCoNiP and placed in a muffle furnace for pre-oxidation treatment, heated at a rate of 3 °C/min to 230 °C for 2 hours, and labeled as FeCoNiP Pre@NCNFs. A 0.05 g sample of the pre-oxidized spinning fiber was placed in a porcelain boat, wrapped with melamine in a mass ratio of (spinning fiber:melamine) 1:10 using a sand-bury method. The alumina porcelain boat was then transferred to a high-temperature tube furnace, with an Ar/H_2 atmosphere selected. The heat treatment steps were as follows: ramp to 400 °C at a heating rate of 5 °C/min and hold for 2 h, then heat to 900 °C at the same rate and hold for 2 h. The resulting sample was labeled FeCoNiP@NCNFs.

The preparation of samples doped with different transition metals follows a similar procedure to the aforementioned method, with the only modification being the addition of 0.25 mmol of Cr, Mn, Cu, or Mo during the spinning solution preparation process. They are labeled as CrFeCoNiP@NCNFs, MnFeCoNiP@NCNFs, CuFeCoNiP@NCNFs, and MoFeCoNiP@NCNFs, respectively.

2.3. Material characterization

The crystalline phase of the prepared catalysts was analyzed by X-ray diffraction (XRD, Max 2500, Rigaku, Japan). X-ray photoelectron spectroscopy (XPS, Thermo K-Alpha, Thermo Fisher, America) was used to analyze the elemental composition and valence states of the catalysts. The morphology and microstructure were characterized by scanning electron microscopy (SEM, JSM-6360LA, JEOL, Japan), while transmission electron microscopy coupled with an energy dispersive spectrometer (TEM and EDS, FEI TECNAI G2 F20, Thermo Fisher, America) was

employed to examine the microstructure, crystal structure and elemental distribution. Raman spectra were recorded on a Raman spectrometer (DXR2 Raman Microscopy, Thermo Fisher, America).

2.4. Electrochemical measurements

All electrochemical measurements were carried out at room temperature in a three-electrode system using a CHI-660E electrochemical workstation. A glassy carbon electrode (GCE, diameter = 5 mm) loaded with the prepared catalysts was used as the working electrode, a graphite rod as the counter electrode, and a Hg/HgO electrode as the reference electrode. All electrochemical tests were performed in 1.0 M KOH (pH = 14), and all potentials throughout the experiment were converted to the reversible hydrogen electrode (RHE).

The working electrode was prepared as follows: first, 5 mg of catalyst powder was added to a mixed solution of 480 μL of water, 40 μL of Nafion and 480 μL of ethanol, and the catalyst ink was obtained by sonication for 0.5 h so that the powder was uniformly dispersed; in the next step, 60 μL of the prepared ink was loaded onto the glassy carbon electrode in five portions to achieve a loading capacity of 1.5 $mg \cdot cm^{-2}$. Linear scanning voltammetric (LSV) curves were measured with 90% i-R compensation in 1.0 M KOH at a sweep rate of 5 $mV \cdot s^{-1}$ for HER and 2 $mV \cdot s^{-1}$ for OER. Tafel plots were derived from the corresponding LSV curves. Double layer capacitance (C_{dl}) was obtained from CV curves at different scan rates within a non-faradaic potential window of 100 mV. Accelerated durability testing (ADT) was performed by 1000 CV cycles in alkaline media. EIS measurements were conducted over a frequency range of 100 kHz to 0.1 Hz with an AC amplitude of 5 mV, and the applied potentials were -0.2 V for HER and 1.6 V for OER (vs. RHE). Long-term stability tests were carried out by the chronopotentiometric method at 10 $mA \cdot cm^{-2}$ to assess the stability of the catalysts in alkaline electrolytes.

3. Results and discussion

FeCoNiP@NCNFs and MFeCoNiP@NCNFs (M = Cr/Mn/Mo/Cu) were all prepared via a simple two-step process. Specifically, the FeCoNiP and high-entropy

phosphide nanoparticles were synthesized using metal salts and phytic acid, while polyacrylonitrile (PAN) was employed to form the carbon nanofiber skeleton and melamine ($C_3H_6N_6$) to construct the nitrogen-doped carbon coating.

3.1. Morphological and structural characterization

The microstructure and morphology of as-prepared catalysts were first observed by field emission scanning electron microscopy (FE-SEM) and transmission electron microscopy (TEM). As shown in Fig. S1, the SEM images of as-spun precursor nanofibers for FeCoNiP@NCNFs, CuFeCoNiP@NCNFs, MnFeCoNiP@NCNFs, and MoFeCoNiP@NCNFs present a similar appearance with the overall structure of the membrane is a cross-linked three-dimensional structure with a smooth surface. Fig. 1a-c show SEM images of CrFeCoNiP@NCNFs at different stages. The doping of metal element Cr did not affect the formation of the three-dimensional skeleton of nanofibers, and there was no significant fracture collapse. In the spinning stage, the overall fiber skeleton is in a highly cross-linked state, and the phosphide nanoparticles are encapsulated inside the carbon nanofibers without being exposed on the fiber surface, confirming the carbon encapsulation structure. CrFeCoNiP@NCNFs was obtained after exposure to 900 °C high temperature. Due to the carbonization of PAN and the formation of the alloy, the catalyst exhibits a slightly larger diameter, resulting in the presence of numerous carbon nanotubes on the surface, which gives the surface a mildly rough texture. Fig. 1 d-g show high-resolution transmission electron microscopy (HRTEM) images, indicating that the surface of the carbon nanofiber matrix is almost smooth and does not have a significant graininess. Clear and continuous lattice stripes can be observed in Fig. 1f, with a measured lattice spacing of 0.183 nm, indicating good crystallinity of the synthesized product. This carbon shell encapsulated phosphide nanoparticle structure not only effectively protects high-entropy phosphide particles from corrosion in harsh environments, but also enhances the electrocatalytic activity of the carbon surface due to the partial electron transfer of the coated phosphide.

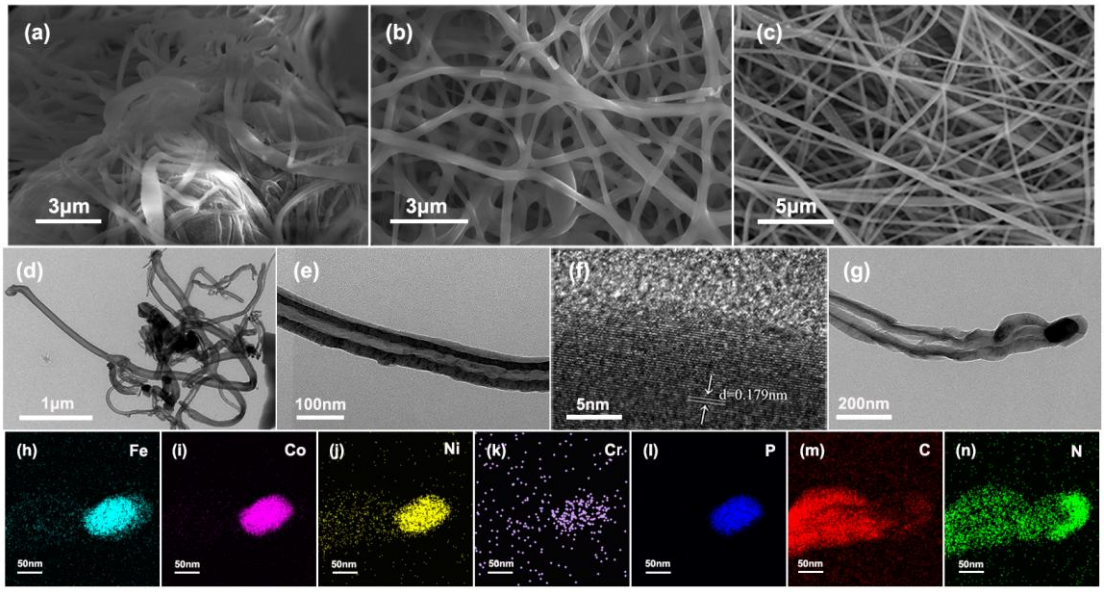


Fig. 1. (a-c) SEM images of the spinning precursor, pre-oxidation at 230°C, and high-temperature sintering at 900 °C for CrFeCoNiP@NCNFs. (d-g) HRTEM images and (h-n) EDS elemental mapping images of CrFeCoNiP@NCNFs.

Fig. 1h-n is the corresponding EDS elemental mapping images, which shows Fe, Co, Ni, Cr, P, C, and N elements in sequence. The high overlap of Cr, Fe, Co, Ni, and P signals in the nanoparticle region indicates that Fe, Co, Ni, Cr, and P multi-component elements are uniformly distributed within the particles, successfully constructing a high entropy phosphide structure. And the N element signal is uniformly distributed in the carbon carrier region, confirming the successful doping of nitrogen element into the carbon skeleton. The aforementioned morphological and elemental characterization results collectively confirm the successful preparation of a multicomponent elemental electrocatalyst, CrFeCoNiP@NCNFs, featuring uniform distribution and excellent particle dispersion.

Fig. 2 presents the XRD spectra of CrFeCoNiP@NCNFs, CuFeCoNiP@NCNFs, MnFeCoNiP@NCNFs, MoFeCoNiP@NCNFs, and FeCoNiP@NCNFs. The phase structure of the catalysts obtained through X-ray diffraction reveals that all samples exhibit broadened diffraction peaks near $2\theta \approx 25$, attributed to the amorphous carbon (002) plane in the NCNFs. The high entropy effect occurred, and multiple metal atoms were doped into the phosphide lattice, causing lattice distortion. As a result, the

diffraction peaks showed slight shifts and broadening, no longer corresponding to a single metal phosphide, proving the formation of high entropy phosphides rather than a simple mixture of multiple metal phosphides. Compared with FeCoNiP@NCNFs, the introduction of Cr/Mn/Mo/Cu elements resulted in changes in the diffraction peaks, indicating that the hetero-metal elements were successfully doped into the crystal lattice.

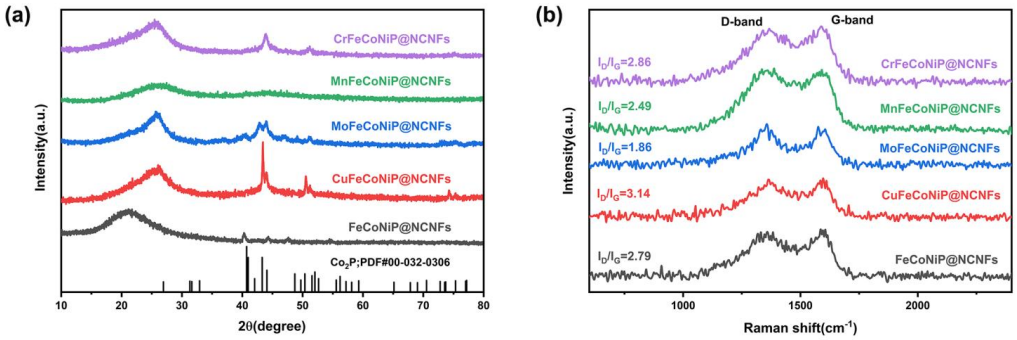


Fig. 2. (a) XRD patterns, (b) Raman spectra of FeCoNiP@NCNFs and MFeCoNiP@NCNFs (M = Cr/Mn/Mo/Cu).

Doping with heteroatoms (Cr/Mn/Mo/Cu) introduces more carbon defects, which can serve as active sites for water electrolysis and promote charge transfer. The defect concentration of Cu doped samples is the highest, while the graphitization degree of Mo doped samples is relatively higher. The defect sites of carbon nanofibers can not only anchor high entropy phosphide particles, but also optimize the adsorption energy of intermediates and enhance the electrocatalytic water splitting performance.

To investigate the chemical composition and elemental valence states on the sample surface, XPS measurements were also performed. The Fe 2p XPS spectrum in Fig. 3 likewise displays four peaks. The two weak peaks at 709.6 eV and 722.7 eV correspond to metallic Fe, while the two peaks at 712 eV and 726 eV are attributed to the oxidized state of Fe species. The P 2p spectra mainly exhibit two sets of peaks in all analyses. The peak at 133.7 eV is mainly caused by the oxidation of P in air. In Fig. 3c, the peaks at 778.3 eV and 793.5 eV correspond to the $Co^{\delta+}$ valence state in Co–P compounds, whereas the peaks at 782.4 eV and 798.1 eV are assigned to the characteristic Co $2p_{1/2}$ and Co $2p_{3/2}$ peaks of oxidized Co species, and the two peaks at 786.7 eV and 802.6 eV correspond to the satellite peaks of Co. As shown in Fig. 3d,

in the high-resolution Ni 2p spectrum of CrFeCoNiP@NCNFs, the Ni $2p_{3/2}$ and Ni $2p_{1/2}$ regions can be fitted into six peaks. The two peaks at 853.2 eV and 870 eV correspond to metallic Ni, the other two peaks at 855.2 eV and 873.2 eV correspond to oxidized Ni, and the remaining two peaks at 861.9 eV and 879.1 eV are satellite peaks.

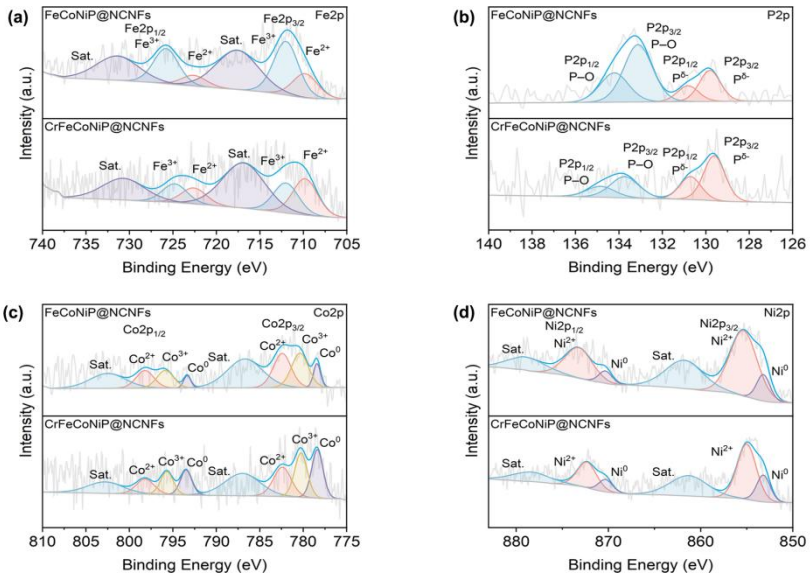


Fig. 3. High resolution XPS spectra of (a) Fe 2p, (b) P 2p, (c) Co 2p, and (d) Ni 2p of CrFeCoNiP@NCNFs and FeCoNiP@NCNFs.

3.2. Electrocatalytic HER performance

HER electrocatalytic performance was evaluated in 1.0 M KOH using a standard three-electrode setup (Fig. 4). Fig. 4a presents iR-compensated LSV curves collected at 5 $mV \cdot s^{-1}$ for as-prepared samples. CrFeCoNiP@NCNFs delivers an overpotential of only 133 mV at 10 $mA \cdot cm^{-2}$. In comparison, FeCoNiP@NCNFs, CuFeCoNiP@NCNFs, MnFeCoNiP@NCNFs, and MoFeCoNiP@NCNFs require 355 mV, 300 mV, 320 mV, and 304 mV, respectively, to reach the same current density. These results demonstrate that CrFeCoNiP@NCNFs possesses substantially enhanced HER activity relative to the undoped FeCoNiP@NCNFs and other doped analogues. Incorporation of Cr into the high-entropy-phosphide lattice generates multivalent cations with complex electronic configurations and improved conductivity and introduces additional phosphorus vacancies. These factors lower the proton-adsorption kinetic barrier and facilitate H-H bond formation. Therefore, the

optimized electronic structure accounts for the prominent HER improvement after Cr doping. Tafel-slope analysis was conducted via the Tafel equation $\eta = a + b \log|j|$ to understand reaction kinetics (Fig. 4b). The Tafel slopes are calculated as 134.68 $mV \cdot dec^{-1}$ (CrFeCoNiP@NCNFs), 144.11 $mV \cdot dec^{-1}$ (MoFeCoNiP@NCNFs), 141.15 $mV \cdot dec^{-1}$ (CuFeCoNiP@NCNFs), 180.98 $mV \cdot dec^{-1}$ (MnFeCoNiP@NCNFs), and 191.4 $mV \cdot dec^{-1}$ (FeCoNiP@NCNFs). The smallest Tafel slope obtained for CrFeCoNiP@NCNFs indicates fast HER kinetics, originating from nanosize effects, the high-entropy effect, and synergistic coupling between Cr and host metal sites. Fig. 4c compares overpotentials at different current densities and confirms that CrFeCoNiP@NCNFs exhibits the lowest overpotential values.

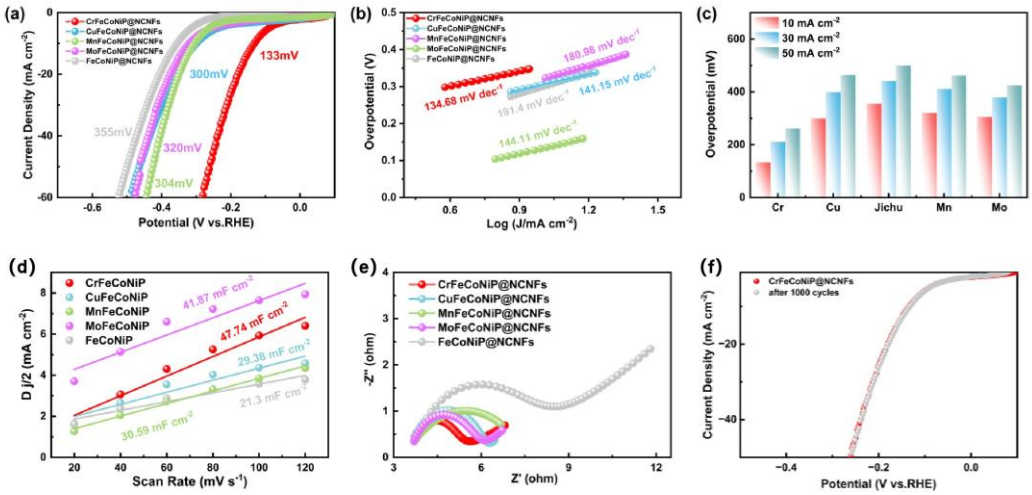


Fig. 4. (a) HER polarization curves with 90% iR compensation and (b) corresponding Tafel slopes. (c) Overpotentials comparison for HER. (d) C_{dl} and (e) EIS of FeCoNiP@NCNFs and MFeCoNiP@NCNFs (M = Cr/Mn/Mo/Cu). (f) LSV curves measured for CrFeCoNiP@NCNFs before and after 1000 CV cycles.

To gain mechanistic insights into HER enhancement, ECSA data were collected from CV tests at different scan rates (Fig. S4) and further processed to produce Fig. 4d. A higher signifies a larger electrochemically active surface area and generally better catalytic activity. CrFeCoNiP@NCNFs achieves the largest C_{dl} value of 47.74 $mF \cdot cm^{-2}$, followed by MoFeCoNiP@NCNFs (41.87 $mF \cdot cm^{-2}$), MnFeCoNiP@NCNFs (30.59 $mF \cdot cm^{-2}$), CuFeCoNiP@NCNFs (29.38 $mF \cdot cm^{-2}$), and FeCoNiP@NCNFs (21.30 $mF \cdot cm^{-2}$). This confirms that Cr doping generates more accessible active sites

and thereby promotes HER activity. Furthermore, the EIS Nyquist plot (Fig. 4e) shows the smallest semicircle for CrFeCoNiP@NCNFs, corresponding to minimum charge-transfer resistance. LSV curves collected before and after 1000 CV cycles nearly overlap (Fig. 4f), verifying favorable HER kinetics and robust durability.

3.3. Electrocatalytic OER performance

Encouraged by the excellent HER performance, the electrocatalytic OER performance of the prepared catalysts was evaluated in 1.0 M KOH solution (Fig. 5). Fig. 5a illustrates the LSV curves of FeCoNiP@NCNFs, CrFeCoNiP@NCNFs, CuFeCoNiP@NCNFs, MnFeCoNiP@NCNFs and MoFeCoNiP@NCNFs. It is evident that the OER activity is markedly enhanced by the incorporation of Cr, and CrFeCoNiP@NCNFs exhibits the most optimal oxygen evolution performance. Fig. 5b shows the corresponding Tafel slope plots derived from the LSV curves for the evaluation of OER kinetics. The Tafel slope of CrFeCoNiP@NCNFs is 45 $mV \cdot dec^{-1}$, which is significantly smaller than that of MoFeCoNiP@NCNFs (55 $mV \cdot dec^{-1}$), CuFeCoNiP@NCNFs (65 $mV \cdot dec^{-1}$), MnFeCoNiP@NCNFs (75 $mV \cdot dec^{-1}$) and FeCoNiP@NCNFs (95 $mV \cdot dec^{-1}$), indicating that it has efficient OER kinetics. In Fig. 5c, at a current density of 10 $mA \cdot cm^{-2}$, the overpotentials of CrFeCoNiP@NCNFs, CuFeCoNiP@NCNFs, MnFeCoNiP@NCNFs, MoFeCoNiP@NCNFs and FeCoNiP@NCNFs are 309 mV, 317 mV, 339 mV, 312 mV and 370 mV, respectively. In addition, their performances at different current densities were analyzed. At a current density of 30 $mA \cdot cm^{-2}$, the overpotential of CrFeCoNiP@NCNFs is 320 mV, which is lower than that of CuFeCoNiP@NCNFs (350 mV), MnFeCoNiP@NCNFs (381 mV), MoFeCoNiP@NCNFs (411 mV) and FeCoNiP@NCNFs (418 mV). Even when the current density reaches 50 $mA \cdot cm^{-2}$, CrFeCoNiP@NCNFs still exhibits the lowest overpotential among these samples, showing the best OER activity.

Furthermore, the C_{dl} derived from the cyclic voltammetry (CV) curves indicates (Fig. 5d) that the C_{dl} of CrFeCoNiP@NCNFs (15.2 $mF \cdot cm^{-2}$) is larger than that of CuFeCoNiP@NCNFs (7.5 $mF \cdot cm^{-2}$), MnFeCoNiP@NCNFs (5.3 $mF \cdot cm^{-2}$), MoFeCoNiP@NCNFs (3.9 $mF \cdot cm^{-2}$) and FeCoNiP@NCNFs (2.3 $mF \cdot cm^{-2}$), owing to the synergistic effect between Cr and the host metals to generate more active sites,

suggesting that Cr introduction can effectively increase the active area, expose more active sites and promote charge transport, thus significantly improving the OER performance. Electrochemical impedance spectroscopy (EIS) was utilized to probe the electron transfer kinetics at the interface. Fig. 5f shows the Nyquist curves of the catalysts. Obviously, the relatively lower resistance of CrFeCoNiP@NCNFs compared to the base FeCoNiP@NCNFs and the other doped samples suggests that the introduced Cr atoms are conducive to promoting electron transfer, which implies a higher charge transfer rate and facilitates the electrocatalytic oxygen evolution reaction. In Fig. 5e, the LSV curves reveal only negligible variations for CrFeCoNiP@NCNFs after 1000 CV cycles, with no obvious degradation in catalytic performance. The LSV curves of other doped catalysts also nearly overlap before and after cycling. These results demonstrate that CrFeCoNiP@NCNFs exhibits outstanding catalytic activity and long-term durability toward the OER.

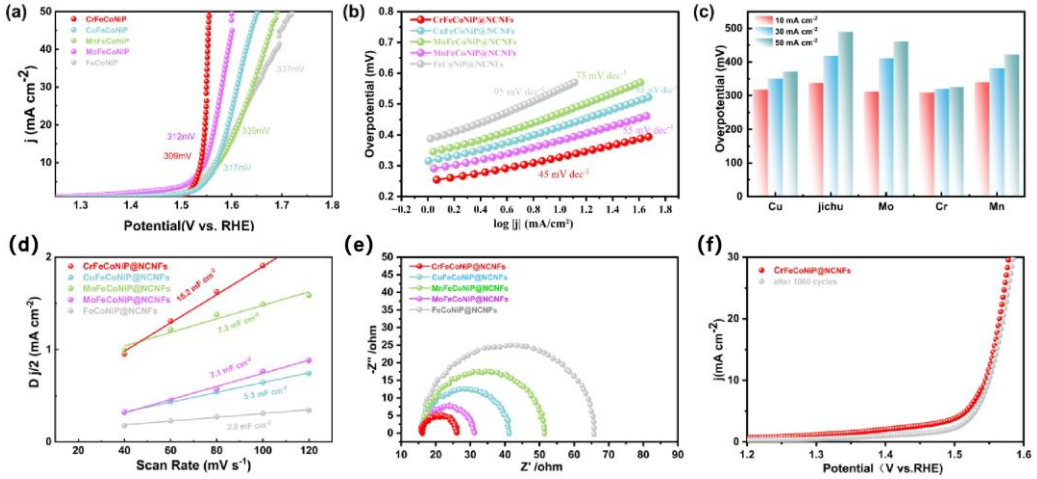


Fig. 5. (a) OER polarization curves with 90% iR compensation and (b) corresponding Tafel slope. (c) Overpotentials comparison for OER. (d) C_{dl} and (e) EIS of FeCoNiP@NCNFs and MFeCoNiP@NCNFs (M = Cr/Mn/Mo/Cu). (f) LSV curves of CrFeCoNiP@NCNFs before and after 1000 CV cycles.

3.4. Overall water splitting

Given the excellent bifunctional activity of CrFeCoNiP@NCNFs, we further tested the overall water splitting performance of CrFeCoNiP@NCNFs as both anode and cathode using a two-electrode system in 1.0 M KOH. The polarization curve (Fig.

6a) shows that CrFeCoNiP@NCNFs only required a cell voltage of 1.89 V to drive a current density of 10 mA·cm^{-2} in alkaline medium. Further chronopotentiometry tests were performed at a current density of 10 mA·cm^{-2}, as shown in Fig. 6b; the obtained potential remained essentially stable during continuous electrolysis, with only a slight gradual increase and no abrupt rise or fall, indicating the good long-term stability of the system.

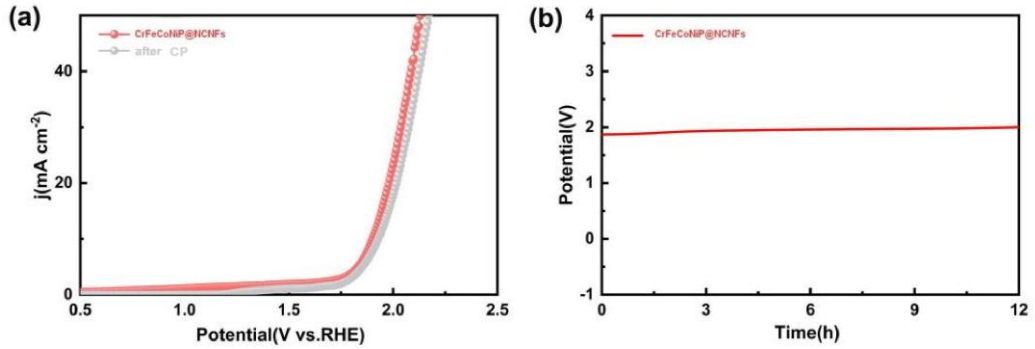


Fig. 6. Electrochemical performance of CrFeCoNiP@NCNFs for overall water splitting in a two-electrode system. (a) Polarization curves. (b) Constant current stability test.

4. Conclusion

In conclusion, we successfully synthesized carbon nanofiber-encapsulated high-entropy phosphides via electrospinning and subsequent thermal treatment using phytic acid as a green, non-toxic phosphorus source. The obtained CrFeCoNiP@NCNFs catalysts exhibit highly efficient and robust electrocatalytic performance for both HER and OER, owing to the increase in electrochemically active area and exposed active sites, the decrease in charge transfer resistance, and the redistribution of charge density induced by the high-entropy effect together with transition-metal. The overall water splitting performance also displays remarkable durability and high efficiency, requiring only a cell voltage of 1.89 V to deliver 10 mA·cm^{-2} while maintaining stable operation for 12 h. The present work elucidates the regulation mechanism of high-entropy phosphides and proposes a green synthesis method for nano-sized phosphides, which is conducive to promoting the practical application of phosphide electrocatalysts.

Acknowledgements

The authors appreciate the Jiangsu Provincial Natural Science Foundation (No. BK20240972), Changzhou Sci & Tech Program (No. CJ20250053), Key project of Jiangsu Provincial Basic Research Program (No. BK20243032) for supporting our work.

References

[1]Quan L, Jiang H, Mei G (2024) Bifunctional electrocatalysts for overall and hybrid water splitting. Chem Rev 124:3694-3812. https://doi.org/10.1021/acs.chemrev.3c00332.

[2]Lee Y, Jeong W, Hwang Y J (2024) Basics, developments, and strategies of transition metal phosphides toward electrocatalytic water splitting: beyond noble metal catalysts. J Mater Chem A 12:28574-28594. https://doi.org/10.1039/d4ta04455j.

[3]Zhang W, Chen Y, Ma Z (2024) Challenges and strategies of transition metal phosphides applied in oxygen evolution reaction of electrocatalytic water splitting: A review. Fuel 369:131741. https://doi.org/10.1016/j.fuel.2024.131741.

[4]Liu L, Liu Y, Liu C (2020) Enhancing the understanding of hydrogen evolution and oxidation reactions on pt (111) through ab initio simulation of electrode/electrolyte kinetics. J Am Chem Soc 142:4985-4989. https://doi.org/10.1021/jacs.9b13694.

[5]Aziz T, Haque M A, Saha S (2023) A review of nanostructured transition metal phosphide-driven electrocatalytic oxygen evolution reaction. Energy Fuels 37:18291-18309. https://doi.org/10.1021/acs.energyfuels.3c02773.

[6]Jing C, Hong L, Li B (2024) A review with transition-metal phosphide electrocatalysts in hydrogen evolution reaction: Doping perspective. Mol Catal 554:113832. https://doi.org/10.1016/j.molcata.2024.113832.

[7]Bai H, Chen D, Ma Q (2022) Atom doping engineering of transition metal phosphides for hydrogen evolution reactions. Electrochem Energy Rev 5:24. https://doi.org/10.1007/s41918-022-00161-7.

[8]Liu B, Lan X, Zhong Q (2024) Metal phosphide: an atypical catalytic site. ACS Catal 14:757-775. https://doi.org/10.1021/acscatal.3c05160.

[9]Yan X, Jia Y, Yao X (2021) Defective structures in metal compounds for energy-related electrocatalysis. Small Struct 2:2000067. https://doi.org/10.1002/sstr.202000067.

[10]Liu Y, Wu Y, Chen X (2026) Metal sulfide-based electrocatalysts for water splitting: From rational design to advanced applications. Fuel 404:136208. https://doi.org/10.1016/j.fuel.2025.136208.

[11]Zhang J, Fu X, Kwon S (2025) Tantalum-stabilized ruthenium oxide electrocatalysts for industrial water electrolysis. Science 387:48-55. https://doi.org/10.1126/science.ado9938.

[12]Huang R, Wen Y, Peng H (2022) Improved kinetics of oer on Ru-Pb binary electrocatalyst by decoupling proton-electron transfer. Chin J Catal 43:130-138. https://doi.org/10.1016/s1872-2067(21)63856-1.

[13]Huang Y, Qin Y, Ye Q (2025) Constructing asymmetric ir-o-ru unit to promote rapid deprotonation and stable lattice oxygen in pbIrRu pyrochlores for water oxidation. Adv Energy Mater 15:2501860. https://doi.org/10.1002/aenm.202501860.

[14]Fan J, Xia J, Wang H (2025) Unveiling the role of single atomic ruthenium decorated cactus-like bimetallic phosphides for alkaline water electrolysis. Adv Energy Mater 15:2501995. https://doi.org/10.1002/aenm.202501995.

[15]Chen D, Pu Z, Lu R (2020) Ultralow ru loading transition metal phosphides as high-efficient bifunctional electrocatalyst for a solar-to-hydrogen generation system. Adv Energy Mater 10:2000814. https://doi.org/10.1002/aenm.202000814.

[16]Sher Shah M S A, Jang G Y, Zhang K (2023) Transition metal carbide-based nanostructures for electrochemical hydrogen and oxygen evolution reactions. EcoEnergy 1:344-374. https://doi.org/10.1002/ece2.18.

[17]Raj G, Das D, Sarkar B (2022) Universal avenue to metal-transition metal carbide grafted N-doped carbon framework as efficient dual Mott-Schottky electrocatalysts for water splitting. Sustain Mater Technol 33:e00451. https://doi.org/10.1016/j.susmat.2022.e00451.

[18]Li C, Zhang Z, Zhu K (2025) Nanoconfined impulse synthesis of high-entropy nanocarbides for active and stable electrocatalysis. Nat Synth 4:1422-1434. https://doi.org/10.1038/s44160-025-00854-z.

[19]Batool M, Hameed A, Nadeem M A (2023) Recent developments on iron and nickel-based transition metal nitrides for overall water splitting: A critical review. Coord Chem Rev 480:215029. https://doi.org/10.1016/j.ccr.2023.215029.

[20]Jayaraman V, Forzanini L, Arumugam L S (2026) Amorphous Iron Vanadium on Anti-Perovskite Nickel Zinc Nitride as an Electrocatalyst for Water-Splitting. Small 22:e13183. https://doi.org/10.1002/smll.202513183.

[21]Zhao Y, Li J, Li K (2025) The synergistic effect of Ni–$NiMo_4N_5$ heterointerface construction and Fe-doping enables active and durable alkaline water/seawater splitting. J Mater Chem A 13:9184-9191. https://doi.org/10.1039/d5ta00038f.

[22]Zuo P, Li N, Lu J (2025) Engineering long-lasting electron buffer of nanoalloys toward overall water splitting of nitrides. ACS Sustain Chem Eng 13:21914-21926. https://doi.org/10.1021/acssuschemeng.5c06945.

[23]Zhao M, Li W, Li J (2020) Strong electronic interaction enhanced electrocatalysis of metal sulfide clusters embedded metal-organic framework ultrathin nanosheets toward highly efficient overall water splitting. Adv Sci 7:2001965. https://doi.org/10.1002/advs.202001965.

[24]Huang Z, Yang Z, Jia Q (2022) Bimetallic Co–Mo sulfide/carbon composites derived from polyoxometalate encapsulated polydopamine-decorated ZIF nanocubes for efficient hydrogen and oxygen evolution. Nanoscale 14:4726-4739. https://doi.org/10.1039/d1nr07913a.

[25]Wang F, Shifa T A, Zhan X (2015) Recent advances in transition-metal dichalcogenide based nanomaterials for water splitting. Nanoscale 7:19764-19788. https://doi.org/10.1039/c5nr06718a.

[26]Hausmann J N, Menezes P W (2022) Why should transition metal chalcogenides be investigated as water splitting precatalysts even though they transform into (oxyhydr)oxides. Curr Opin Electrochem 34:100991. https://doi.org/10.1016/j.coelec.2022.100991.

[27]Huang L, Gao R, Qiu Y (2025) In situ reconfigured heterostructure active sites on transition metal sulfides heterojunction for accelerated water oxidation. Inorg Chem 64:9703-9714. https://doi.org/10.1021/acs.inorgchem.5c00902.

[28]Zhang B, Zhao Y, Li X (2025) Rapidly reconstructed $CuCo_2S_4$ @Co–V–O–F nanocatalysts for efficient and stable overall water splitting in alkaline and seawater electrolysis. RSC Adv 15:19443-19455. https://doi.org/10.1039/d5ra03052h.

[29]Oyama S T (2003) Novel catalysts for advanced hydroprocessing: transition metal phosphides. J Catal 216:343-352. https://doi.org/10.1016/s0021-9517(02)00069-6.

[30]Chen M, Guan J (2024) Achievements and challenges in cobalt-based catalysts for water electrolysis. Chem Eng J 500:157080. https://doi.org/10.1016/j.cej.2024.157080.

[31]Tong J, Xing Y, Xiao X (2024) Iron-doped cobalt phosphide nanowires prepared via one-step solvothermal phosphidization of metal–organic frameworks for the oxygen evolution reactions. Green Chem 26:5308-5325. https://doi.org/10.1039/d4gc00132j.

[32]Wu J, Wang D, Wan S (2022) An efficient cobalt phosphide electrocatalyst derived from cobalt phosphonate complex for all-pH hydrogen evolution reaction and overall water splitting in alkaline solution. Small 18:2202883. https://doi.org/10.1002/smll.202202883.

[33]Maity C K, Roy S, Adhikari A D (2025) Mixed transition metal phosphides: recent progress and frontiers in secondary batteries and supercapacitors. Nanoscale 17:22050-22085. https://doi.org/10.1039/d5nr01892g.

[34]Zhang H-M, Zuo L, Gao Y (2024) Amorphous high-entropy phosphoxides for efficient overall alkaline water/seawater splitting. J Mater Sci Technol 173:1-10. https://doi.org/10.1016/j.jmst.2023.08.003.

[35]Jiang L, Jiang L, Luo X (2024) Iron-Induced vacancy and electronic regulation of nickle phosphides for ampere-level alkaline water/seawater splitting. Chem Eng J 502:157952. https://doi.org/10.1016/j.cej.2024.157952.

[36]Zhang Y, Zhang M, Zhang H (2025) Bimetallic Mn and Cr co-doped nickel cobalt phosphide nanoneedle arrays as bifunctional electro catalysts for overall water splitting. Fuel 396:135348. https://doi.org/10.1016/j.fuel.2025.135348.

[37]Cai Z-X, Goou H, Ito Y (2021) Nanoporous ultra-high-entropy alloys containing fourteen elements for water splitting electrocatalysis. Chem Sci 12:11306-11315. https://doi.org/10.1039/d1sc01981c.

[38]Zhang H, Zhang Q, Zeng X (2024) Construction of multiple heterogeneous interfaces and oxygen evolution reaction of hollow CoFe bimetallic phosphides derived from MOF template. Prog Nat Sci-Mater Int 34:913-920. https://doi.org/10.1016/j.pnsc.2024.09.001.

[39]Sun X, Wei P, Zhang J (2021) P, N-codoped carbon nanofibers confined ultra-small bimetallic NiCoP for highly efficient overall water splitting. Appl Surf Sci 570:151247. https://doi.org/10.1016/j.apsusc.2021.151247.

Supplementary Files

This is a list of supplementary files associated with this preprint. Click to download.

- SupportingInformationforPublication.docx